ChemComm

COMMUNICATION

View Article Online
View Journal | View Issue

Cite this: *Chem. Commun.*, 2017, 53, 3741

Received 23rd January 2017,
Accepted 6th March 2017

DOI: 10.1039/c7cc00627f

rsc.li/chemcomm

The structure and opto–thermo electronic properties of a new $(Bi(Bi_2S_3)_9I_3)_{2/3}$ hexagonal nano-/micro-rod†

Ching-Hwa Ho,*[a] Ya-Han Chen,[a] Yung-Kang Kuo[b] and C. W. Liu[c]

The semiconductor optoelectronic properties of an inorganic $(Bi(Bi_2S_3)_9I_3)_{2/3}$ hexagonal nano-/micro-rod are firstly explored herein. Transmittance and thermoreflectance measurements show that $(Bi(Bi_2S_3)_9I_3)_{2/3}$ hexagonal rods possess an indirect gap of 0.73 eV and a direct gap of 1.08 eV, respectively. Hot-probe measurements of $(Bi(Bi_2S_3)_9I_3)_{2/3}$ reveal the p-type semiconductor behavior and high thermoelectric voltage. Polarized Raman measurements of the *m*-plane $(Bi(Bi_2S_3)_9I_3)_{2/3}$ (along *c* and perpendicular to the *c* axis) identify the structural anisotropy of the hexagonal nano-/micro-rod.

Bi_2X_3 (X = S, Se, Te) are group V–VI semiconductors which belong to a family of renowned thermoelectric materials used in thermal-electric power production. For thermoelectric materials, the efficiency is determined by a dimensionless figure of merit (*ZT*), defined as $ZT = S^2 \cdot T/(\rho \cdot \kappa)$, where *S*, ρ, *T* and κ are the Seebeck coefficient, electrical resistivity, absolute temperature and thermal conductivity, respectively.[1] Among the Bi_2X_3 compounds, Bi_2Se_3, Bi_2Te_3, and their alloys Bi_2Se_3–Bi_2Te_3 possess high efficiency at a *ZT* value from 0.4 to 1.0 at room temperature,[2–4] whereas Bi_2S_3 has generally a maximum *ZT* value lower than 0.1 at 300 K.[5] The proper use of a dopant inside the Bi_2X_3 compound can improve the thermoelectric behaviour of the alloy. A Sb doped Bi–Te alloy can reach a highest *ZT* value of 1.86 ± 0.15 at 320 K.[6] Bi_2S_3 doped with 0.5 mol% $CuBr_2$ attains a high *ZT* of 0.72 at 773 K.[7] The undoped Bi_2S_3 essentially possesses lower *ZT* than those of Bi_2Se_3 and Bi_2Te_3 but it is nontoxic (green) and low cost (abundant) for renewable energy source applications. The *ZT* difference appears partly because Bi_2Se_3 and Bi_2Te_3 possess a rhombohedral structure[8,9] and a topological-insulator interface[10] while Bi_2S_3 belongs to the orthorhombic crystalline phase.[8,11,12] The difference between the crystal structures of Bi_2S_3 and Bi_2X_3 (X = Se and Te) may influence the thermo-electric efficiency, however, the larger band gap of bismuth sulfide approaching 1 eV[13,14] can make Bi_2S_3 suitable for use in solar-energy conversion.

In this study, the optical and electrical properties of a new semiconductor $(Bi(Bi_2S_3)_9I_3)_{2/3}$ hexagonal rod have been evaluated using temperature-dependent transmittance, thermoreflectance (TR), and electrical conductivity measurements. The $(Bi(Bi_2S_3)_9I_3)_{2/3}$ hexagonal nano-/micro-rods have been grown by the chemical vapour transport (CVT) method. High-resolution transmission electron microscopy (HRTEM) and X-ray diffraction (XRD) measurements confirm the hexagonal phase of the as-grown crystals, and energy dispersive X-ray (EDX) spectroscopy and small single crystal XRD identify the stoichiometry of the crystals. From the experimental results of transmittance and TR, the $(Bi(Bi_2S_3)_9I_3)_{2/3}$ [$\sim(Bi(Bi_2S_3)_9I_3)_{0.667}$] compound is confirmed to be an indirect semiconductor, possessing an indirect optical gap E_g^{ind} = 0.73 ± 0.03 eV and a direct gap E_g^{d} = 1.08 ± 0.02 eV, respectively. Although a very small amount of bismuth sulphide iodide (BiSI) has ever been reported, the stoichiometric content of the compound cannot be well defined and the crystal structure is not the hexagonal type [*i.e.* it is orthorhombic].[15,16] The crystalline phase of the hexagonal $(Bi(Bi_2S_3)_9I_3)_{0.667}$ has been investigated using XRD,[17,18] however, its material properties have not been explored. According to our hot-probe measurements, the carrier type of the hexagonal $(Bi(Bi_2S_3)_9I_3)_{0.667}$ nano-/micro-rod possesses p-type conductivity. The Bi_2S_3 crystal generally reveals degenerate n-type carrier conduction due to the existence of abundant sulphur vacancies inside the crystal.[19] The incorporation of iodine inside the hexagonal $(Bi(Bi_2S_3)_9I_3)_{0.667}$ will compensate the sulphur vacancies in Bi_2S_3 (*i.e.* donors) and even results in a p-type acceptor level (A). In this work, the acceptor level A in $(Bi(Bi_2S_3)_9I_3)_{0.667}$ can also be detected by means of temperature-dependent conductivity and TR measurements. Both optical and electrical measurements demonstrate the $(Bi(Bi_2S_3)_9I_3)_{0.667}$ hexagonal rod to be a potential material with dual energy production from solar and thermoelectric power.

[a] *Graduate Institute of Applied Science and Technology, National Taiwan University of Science and Technology, Taipei 106, Taiwan. E-mail: chho@mail.ntust.edu.tw; Fax: +886 2 27303733; Tel: +886 2 27303772*

[b] *Department of Physics, National Dong Hwa University, Shoufeng, Hualien 974, Taiwan*

[c] *Department of Chemistry, National Dong Hwa University, Shoufeng, Hualien 974, Taiwan*

† Electronic supplementary information (ESI) available. See DOI: 10.1039/c7cc00627f

The single crystals of $(Bi(Bi_2S_3)_9I_3)_{0.667}$ hexagonal rods were grown by the CVT method. The compounds of the crystals were prepared from the elements Bi: 99.99% pure, S: 99.999% and I: 99.99%. To achieve stoichiometry, excess iodine was added with respect to the stoichiometric mixture of the constituent elements. Some iodine was used for compound synthesis, and some iodine acted as the transport agent. About 12 g of the elements were introduced into a quartz ampoule (22 mm OD, 17 mm ID, 20 cm length), which was then cooled with liquid nitrogen, evacuated to 10^{-6} Torr and sealed.[20,21] The mixture was slowly heated to 600 °C and maintained for two days. The temperature was then set as 600 °C (heating zone) → 550 °C (growth zone) with a gradient of −2.5 °C cm^{-1} in a horizontal tube furnace. The reaction was carried out for 240 h for producing single crystals. After the growth the as-grown $(Bi(Bi_2S_3)_9I_3)_{0.667}$ crystals obtained a black-shiny surface and a rod-shape outline with a diameter of about hundred nm to hundred μm. The structure and stoichiometric analysis using XRD and energy dispersive X-ray (EDX) are shown in the ESI.† The crystal structure is hexagonal ($P63/m$) and lattice constants are a = 15.71 Å and c = 4.02 Å. The stoichiometric composition is determined to be $Bi_{12.667}S_{18}I_2$, corresponding to $(Bi(Bi_2S_3)_9I_3)_{0.667}$. The experimental details of optical characterization methods are also provided in the ESI.†

Fig. 1(a) shows the HRTEM image, selection-area electron diffraction (SEAD) pattern, and fast Fourier transform (FFT) pattern of a m-plane $(Bi(Bi_2S_3)_9I_3)_{0.667}$ grown by CVT. The crystal morphology of the as-grown $(Bi(Bi_2S_3)_9I_3)_{0.667}$ crystals is shown in the upper part of Fig. 1(b). The outline of the as-grown $(Bi(Bi_2S_3)_9I_3)_{0.667}$ is essentially hexagonal rods with a top hexagon plane. The representative scheme of the crystal plane and crystal orientation for the hexagonal structure is depicted in the lower part of Fig. 1(b), where the m-plane is the side plane of the hexagonal rod. The crystal directions of c, a_1, a_2, and a_3 of the hexagonal structure are also shown. The clear atomic sites of the HRTEM image and dotted SAED patterns displayed in Fig. 1(a) reveal the high crystalline quality of the $(Bi(Bi_2S_3)_9I_3)_{0.667}$ nano rod. The FFT pattern in the lower part of Fig. 1(a) shows the same dotted arrangement as that of the SEAD pattern. It also verifies good crystalline quality of the m-plane $(Bi(Bi_2S_3)_9I_3)_{0.667}$. The lattice constants of hexagonal $(Bi(Bi_2S_3)_9I_3)_{0.667}$ can be determined to be a = 1.57 nm and c = 0.4 nm using the HRTEM image in Fig. 1(a) and the result matches well with that obtained by powder XRD in the ESI.† Fig. 1(c) shows the HRTEM, SEAD, and FFT results of the c-plane $(Bi(Bi_2S_3)_9I_3)_{0.667}$. The clear atomic sites of the HRTEM image and obvious dotted SAED patterns identify the high crystallinity of the c-plane $(Bi(Bi_2S_3)_9I_3)_{0.667}$. The FFT pattern in Fig. 1(c) reveals a hexagonal structure and the lattice spacing of the m-plane [*i.e.* $(10\bar{1}0)$] is estimated to be 1.36 nm.

To further characterize the semiconductor properties of the $(Bi(Bi_2S_3)_9I_3)_{0.667}$ micro rod, TR and transmittance measurements are implemented. TR is proven to be a very effective tool for probing direct interband transitions near critical-point transitions of the semiconductor band structure.[22,23] The derivative line shape of the TR spectral feature suppresses unwanted background and emphasizes the energy position of the direct transition feature.[23] Open-circle lines in Fig. 2(a) and (b) are the

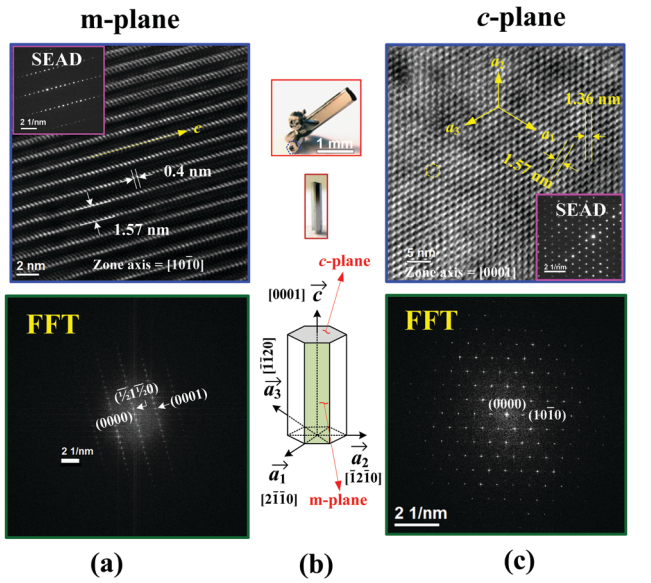

Fig. 1 (a) HRTEM image, SEAD and FFT patterns of the m-plane $(Bi(Bi_2S_3)_9I_3)_{0.667}$. (b) Crystal morphology of the as-grown $(Bi(Bi_2S_3)_9I_3)_{0.667}$ hexagonal rod. The representative scheme of crystal planes and orientations of the hexagonal structure is also included for comparison. (c) HRTEM image, SEAD and FFT patterns of the c-plane $(Bi(Bi_2S_3)_9I_3)_{0.667}$.

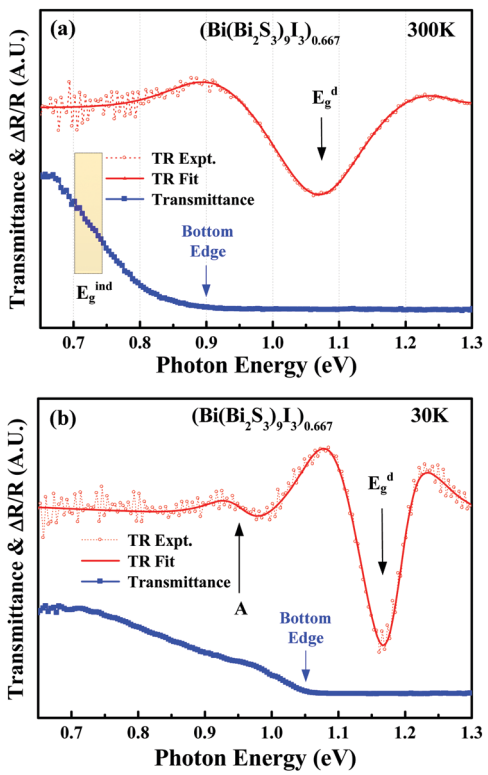

Fig. 2 Thermoreflectance (TR) and transmittance spectra of m-plane $(Bi(Bi_2S_3)_9I_3)_{0.667}$ at (a) 300 K and (b) 30 K. The open-circle lines are the experimental TR data and solid lines are the derivative Lorentzian line-shape fits to the TR spectra. The obtained transition energies (E_g^d and A) from the fits are indicated by arrows.

TR spectra of $(Bi(Bi_2S_3)_9I_3)_{0.667}$ at 300 and 30 K. The solid lines are the least-square fits by using a derivative Lorentzian line-shape function expressed as $\Delta R/R = \mathrm{Re}[\sum A \cdot e^{j\phi}(E - E_g^d + j\Gamma)^{-m}]$,[23] where A and ϕ are the amplitude and phase of the line shape, and E_g^d and Γ are the energy and broadening parameter of the interband transition. The value $m = 0.5$ is used for the first derivative line shape analysis of critical-point transition of the direct band gap for $(Bi(Bi_2S_3)_9I_3)_{0.667}$. The obtained values of the direct band gap E_g^d from the fits in Fig. 2 are 1.08 ± 0.02 eV at 300 K and 1.182 ± 0.008 eV at 30 K, respectively. As the general semiconductor behaviour, as the temperature is decreased, the E_g^d feature of $(Bi(Bi_2S_3)_9I_3)_{0.667}$ in Fig. 2 reveals energy blueshift behaviour and line-shape broadened character owing to the shrinkage of the lattice (*i.e.* shortening in bond length) and reduction in environmental heat (*i.e.* decrease in the thermal lattice vibration). As shown in Fig. 2(b), one more feature ($A = 0.962 \pm 0.008$ eV) can also be detected by TR at 30 K. It may come from an acceptor level caused by iodine incorporation in $(Bi(Bi_2S_3)_9I_3)_{0.667}$. We will discuss the origin of the A feature later. To identify the band-edge character of $(Bi(Bi_2S_3)_9I_3)_{0.667}$, transmittance results at 300 and 30 K are also, respectively, shown in Fig. 2(a) and (b) for comparison. For a direct semiconductor, the transmittance absorption edge must be at approximately the centre of the direct band gap E_g^d.[22] However, for $(Bi(Bi_2S_3)_9I_3)_{0.667}$, the energy position of the transmittance bottom edge (~0.9 eV at 300 K and ~1.05 eV at 30 K) is lower than that of the corresponding E_g^d as shown in Fig. 2. It verifies an indirect absorption edge that existed in $(Bi(Bi_2S_3)_9I_3)_{0.667}$. From Fig. 2(a), the indirect gap of $(Bi(Bi_2S_3)_9I_3)_{0.667}$ is estimated to be about $E_g^{ind} = 0.73 \pm 0.03$ eV at room temperature. The $(Bi(Bi_2S_3)_9I_3)_{0.667}$ hexagonal nano-/micro rod is hence shown to be an indirect semiconductor.

In order to further verify the semiconductor behaviour of the $(Bi(Bi_2S_3)_9I_3)_{0.667}$ hexagonal rod, temperature-dependent conductivity (σ) measurement is implemented. Fig. 3(a) shows the semi-logarithm plot of σ *vs.* reciprocal temperature ($1000/T$) in the temperature range between 20 and 300 K. The conductivity is $\sigma = 9.31 \times 10^{-8}$ S cm^{-1} at 20 K. With an increase in the temperature, the conductivity of $(Bi(Bi_2S_3)_9I_3)_{0.667}$ increases to 9×10^{-4} S cm^{-1} at 300 K. It behaves like a general electrical characteristic of semiconductors. The increase of conductivity with temperature is mostly correlated with the ionization of impurity to provide more conduction carriers in $(Bi(Bi_2S_3)_9I_3)_{0.667}$. The temperature dependence of electrical conductivity in semiconductors can be expressed as $\sigma = \sigma_0 \cdot \exp(\Delta E/kT)$, where ΔE is the activation energy for carriers and k is the Boltzmann constant. From Fig. 3(a), with $T > 200$ K (*i.e.* $1000/T < 5$), the $\ln \sigma$ *vs.* $1000/T$ graph shows the linear region where the slope yields carriers' activation energy $\Delta E = 0.22$ eV for the $(Bi(Bi_2S_3)_9I_3)_{0.667}$ hexagonal rod. Hot probe measurement shows clearly the p-type conduction behaviour for the $(Bi(Bi_2S_3)_9I_3)_{0.667}$ micro rod and we will discuss the experimental results later. The activation energy $\Delta E = 0.22$ eV of $(Bi(Bi_2S_3)_9I_3)_{0.667}$ means an acceptor level may exist in the band gap. Fig. 3(b) shows the representative scheme of the $(Bi(Bi_2S_3)_9I_3)_{0.667}$ hexagonal rod near the band edge which refers to the optical and electrical measurements. The indirect band gap E_g^{ind} is ~0.73 eV and the direct band gap E_g^d is ~1.08 eV at 300 K, which are measured by transmittance and TR. An acceptor level with an activation energy of $\Delta E = 0.22$ eV is located above the valence band (E_V). It can also be verified by the TR experiment at low temperature [*i.e.* the A feature in Fig. 2(b)] with an energy difference of $A = E_g^d - \Delta E = 0.962$ eV, similar to the TR result.

Fig. 4 shows the experimental setup and measurement results of the hot probe measurements for a $(Bi(Bi_2S_3)_9I_3)_{0.667}$ hexagonal rod (size ~0.5 × 0.5 × 8 mm^3). The end contacts of the $(Bi(Bi_2S_3)_9I_3)_{0.667}$ rod were made using silver paste and a metal wire. A solder-iron probe was heated to ~160 °C to act as the hot probe source. When the solder iron comes into contact with the hot end of the $(Bi(Bi_2S_3)_9I_3)_{0.667}$ rod, a negative electro-motive force (thermoelectric power) of $\Delta V = -53.62$ mV can be detected by the rod. In hot probe (thermoelectric probe) measurements, the conductivity type can be determined by the sign of thermal electro-motive force (Seebeck voltage) ΔV by a thermal gradient. The carriers' diffusion current could be dominated by the concentration of excited minority carriers, *i.e.* $\Delta n = (n_{excited} - n_0)$ for the thermally excited electrons in a p-type semiconductor, which is expressed as:[24]

$$J_n = (-q) \cdot \Delta n \cdot \mu_e \cdot P_n \cdot \Delta T/\Delta x \quad (1)$$

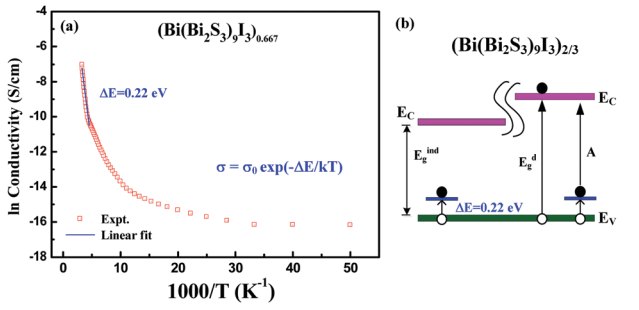

Fig. 3 (a) Temperature-dependent conductivity of a $(Bi(Bi_2S_3)_9I_3)_{0.667}$ hexagonal rod. The solid line in the high-temperature region is a linear fit to obtain activation energy ΔE of conduction carriers. (b) Representative band-edge scheme for $(Bi(Bi_2S_3)_9I_3)_{0.667}$.

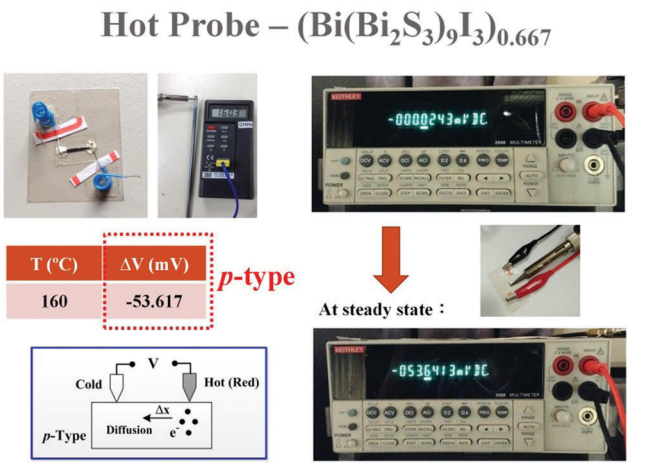

Fig. 4 Experimental setup and measurement results of the hot-probe experiment for a $(Bi(Bi_2S_3)_9I_3)_{0.667}$ hexagonal rod (size ~0.5 × 0.5 × 8 mm^3). The hot-probe source is a solder iron of $T \approx 160$ °C and the Seebeck voltage is measured using a volt meter. The representative scheme of generation of thermally excited minority carriers by the hot probe is also included for comparison.

where $P_n = \Delta V/\Delta T$ is the differential thermoelectric power (Seebeck coefficient), and $\Delta T/\Delta x$ is the temperature gradient between hot and cold probes. Because the measured $\Delta V = -53.62$ mV in Fig. 4 the $(Bi(Bi_2S_3)_9I_3)_{0.667}$ rod is confirmed to be a p-type semiconductor. The Seebeck coefficient obtained using the hot probe experiment is determined to be $|P_n| \approx 397$ μV °C^{-1}. The value is similar to that obtained by traditional thermoelectric measurement (*i.e.* two thermal couples combined with one end heater). The thermal conductivity determined by thermoelectric measurement is ~4.57 W (m °C)$^{-1}$. The Seebeck coefficient of $(Bi(Bi_2S_3)_9I_3)_{0.667}$ is slightly larger than those (50–250 μV °C^{-1}) of Bi_2Se_3 and Bi_2Te_3 determined previously.[4] The optical properties of the band gap approaching 1 eV and the specific characteristic of thermoelectric power generation of the nano-/micro-rod $(Bi(Bi_2S_3)_9I_3)_{0.667}$ make the chalcogenide material a potential candidate for dual-power source production from thermoelectric and solar energy.

Fig. 5 shows polarized micro-Raman (μRaman) spectra of the *m*-plane $(Bi(Bi_2S_3)_9I_3)_{0.667}$ hexagonal micro rod. The measurement configurations include unpolarised, $Z(XX)\bar{Z}$, and $Z(XY)\bar{Z}$ polarization conditions. The orientations are defined as $X = [0001]$, $Y = [\bar{1}2\bar{1}0]$, and $Z = [10\bar{1}0]$, respectively [*i.e.* see the indication in Fig. 1(b)]. Four Raman bands can be detected at about 146, 195, 227, and 266 cm^{-1} in the unpolarised μRaman spectrum in Fig. 5. Specially two prominent Raman peaks at 195 cm^{-1} and 266 cm^{-1} show clear polarization dependence by the selection rule. The 195 cm^{-1} mode is present only in the $Z(XY)\bar{Z}$ polarized condition while the 266 cm^{-1} appears merely along the $Z(XX)\bar{Z}$ linear polarization. The clear polarization dependence of the two dominant modes can also verify the structural anisotropy of the hexagonal rod-shape $(Bi(Bi_2S_3)_9I_3)_{0.667}$ along *c* and perpendicular to the *c* axis such as the outline shape shown in the inset of Fig. 5, and that in Fig. 1(b).

In conclusion, HRTEM, optical, thermoelectric, and Raman results of a new semiconductor $(Bi(Bi_2S_3)_9I_3)_{0.667}$ have been firstly explored. The crystal was successfully grown by the CVT method, and the structure and stoichiometry of the compound were confirmed. The hexagonal nano-/micro-rod of $(Bi(Bi_2S_3)_9I_3)_{0.667}$ reveals an indirect band gap around 0.73 eV and a direct band gap around 1.08 eV. The HRTEM image, SEAD pattern and FFT result verified the hexagonal structure of the rod. The p-type semiconductor behaviour of $(Bi(Bi_2S_3)_9I_3)_{0.667}$ is confirmed by hot probe measurement. The acceptor level's activation energy is determined to be 0.22 eV by temperature-dependent conductivity and low-temperature TR measurements. The Seebeck coefficient and thermal conductivity of $(Bi(Bi_2S_3)_9I_3)_{0.667}$ are 397 μV °C^{-1} and 4.57 W (m °C)$^{-1}$, respectively. Polarized Raman scattering on the *m*-plane rod confirms the structural anisotropy of the rod-shape $(Bi(Bi_2S_3)_9I_3)_{0.667}$, where a prominent 266 cm^{-1} mode appeared merely along the sulphur-atoms' relative vibrations along the *c* axis. The optical, electrical and thermoelectric characteristics of the nano-/micro-rods reveal $(Bi(Bi_2S_3)_9I_3)_{0.667}$ as a promising material for green energy application.

This work was financially supported by the funding from The Ministry of Science and Technology, Taiwan, under grant no. MOST 104-2112-M-011-002-MY3.

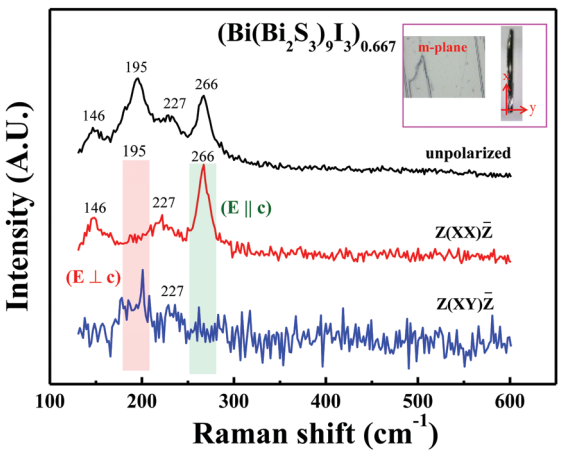

Fig. 5 Polarized Raman spectra of a $(Bi(Bi_2S_3)_9I_3)_{0.667}$ hexagonal micro rod on the *m*-plane with unpolarized, $Z(XX)\bar{Z}$ and $Z(XY)\bar{Z}$. The *X* direction is along the *c* axis of the rod. The *m*-plane morphology and crystal orientations are also shown in the inset for comparison.

Notes and references

1 P. F. P. Poudeu, J. D_Angelo, A. D. Downey, J. L. Short, T. P. Hogan and M. G. Kanatzidis, *Angew. Chem., Int. Ed.*, 2006, **45**, 1–5.
2 M. Saleemi, M. S. Toprak, S. Li, M. Johnsson and M. Muhammed, *J. Mater. Chem.*, 2012, **22**, 725–730.
3 G. L. Sun, L. L. Li, X. Y. Qin, D. Li, T. H. Zou, H. X. Xin, B. J. Ren, J. Zhang, Y. Y. Li and X. J. Li, *Appl. Phys. Lett.*, 2015, **106**, 053102.
4 A. Soni, Z. Yanyuan, Y. Ligen, M. K. K. Aik, M. S. Dresselhaus and Q. Xiong, *Nano Lett.*, 2012, **12**, 1203–1209.
5 Z. H. Ge, B. P. Zhang and J. F. Li, *J. Mater. Chem.*, 2012, **22**, 17589–17594.
6 S. I. Kim, K. H. Lee, H. A. Mun, H. S. Kim, S. W. Hwang, J. W. Roh, D. J. Yang, W. H. Shih, X. S. Li, Y. H. Lee, G. J. Snyder and S. W. Kim, *Science*, 2015, **348**, 109–114.
7 Z. Liu. Y. Pei, H. Geng, J. Zhou, X. Meng, W. Cai, W. Liu and J. Sui, *Nano Energy*, 2015, **13**, 554–562.
8 W. Liu, K. C. Lukas, K. McEnaney, S. Lee, Q. Zhang, C. P. Opeil, G. Chen and Z. Ren, *Energy Environ. Sci.*, 2013, **6**, 552–560.
9 V. V. Sobolevs, D. Shutovy, V. POPOVan and S. N. Shestatsk, *Phys. Status Solidi B*, 1968, **30**, 349–355.
10 H. Zhang, C.-X. Liu, X.-L. Qi, X. Dai, Z. Fang and S.-C. Zhang, *Nat. Phys.*, 2009, **5**, 438–442.
11 J. Tang and A. P. Alivisatos, *Nano Lett.*, 2006, **6**, 2701–2706.
12 V. Calzia, R. Piras, A. Ardu, A. Musinu, M. Saba, G. Bongiovanni and A. Mattoni, *J. Phys. Chem. C*, 2015, **119**, 16913–16919.
13 G. Konstantatos, L. Levina, J. Tang and E. H. Sargent, *Nano Lett.*, 2008, **8**, 4002–4006.
14 W. Lou, M. Chen, X. Wang and W. Liu, *Chem. Mater.*, 2007, **19**, 872–878.
15 D. Arivuoli, F. D. Gnanam and P. Ramasamy, *J. Mater. Sci.*, 1986, **21**, 2835–2842.
16 R. Nitsche and W. J. Merz, *J. Phys. Chem. Solids*, 1960, **13**, 154–155.
17 G. Shen, D. Chen, K. Tang, L. Huang and Y. Qian, *J. Cryst. Growth*, 2003, **249**, 331–334.
18 G. Miehe and V. Kupčík, *Naturwissenschaften*, 1971, **58**, 219.
19 B. Chen, C. Uher, L. Iordanidis and M. G. Kanatzidis, *Chem. Mater.*, 1997, **9**, 1655–1658.
20 C. H. Ho, *J. Mater. Chem.*, 2011, **21**, 10518–10524.
21 C. H. Ho and Y. J. Chu, *Adv. Opt. Mater.*, 2015, **3**, 1750–1758.
22 C. H. Ho, C. H. Lin, Y. P. Wang, Y. C. Chen, S. H. Chen and Y. S. Huang, *ACS Appl. Mater. Interfaces*, 2013, **5**, 2269–2277.
23 D. E. Aspnes, in *Optical properties of solids, Handbook on Semiconductors*, ed. M. Balkanski, North Holland, Amsterdam, 1980, p. 109.
24 D. K. Schroder, in *Semiconductor Material and Device Characterization*, John Wiely & Sons, Inc., Hoboken, NJ, 2006, p. 38.

Supplementary Information

Structure and opto-thermo electronic property of a newly $(Bi(Bi_2S_3)_9I_3)_{2/3}$ hexagonal nano-/micro- rod

Ching-Hwa Ho[a,*] Ya-Han Chen,[a] Yung-Kang Kuo,[b] and C. W. Liu[c]

[a]Graduate Institute of Applied Science and Technology, National Taiwan University of Science and Technology, Taipei 106, Taiwan

[b]Department of Physics, National Dong Hwa University, Shoufeng, Hualien 974, Taiwan

[c]Department of Chemistry, National Dong Hwa University, Shoufeng, Hualien 974, Taiwan

[*]E-mail: chho@mail.ntust.edu.tw

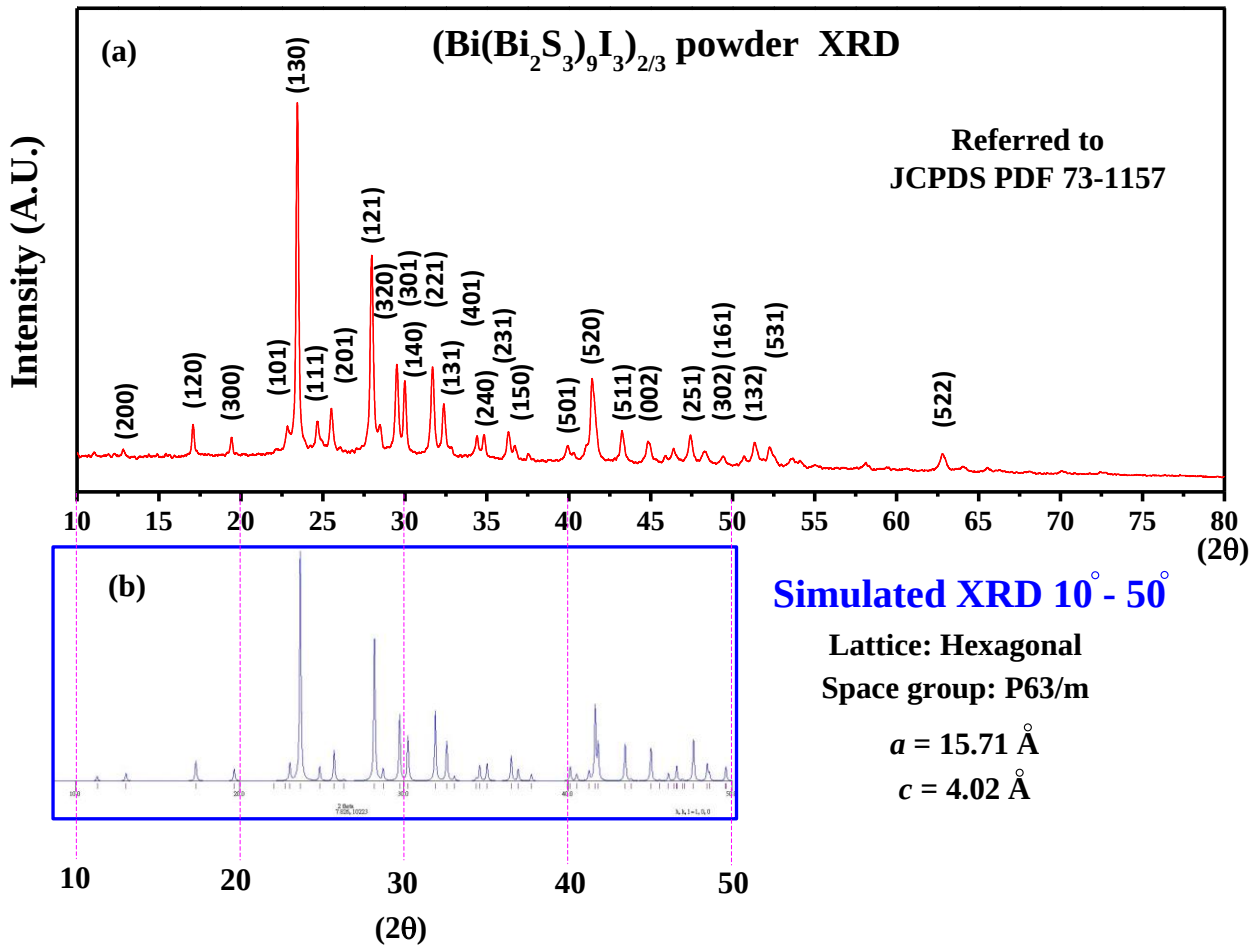

Fig. S1. (a) Experimental X-ray diffraction (XRD) pattern of the $(Bi(Bi_2S_3)_9I_3)_{0.667}$ grown by CVT. The sample preparation is accomplished by finely ground some small crystals of $(Bi(Bi_2S_3)_9I_3)_{0.667}$ into powder, and the powder XRD pattern is taken and recorded by means of a Cu K_α radiation in the 2θ range of 10° - 80°. The peak angle (2θ) and plane index for each of the diffraction peaks are compared and referred to previous JCPDS card No. 73-1157 [18]. The lattice constants determined from the experimental XRD results in (a) are *a*=15.71 Å and *c*=4.02 Å, respectively. The structure of crystal lattice is hexagonal. (b) Simulated XRD curve of $(Bi(Bi_2S_3)_9I_3)_{0.667}$ using the obtained lattice constants and crystal structure from 10° - 50°. The relative intensities and peak positions of the simulated XRD pattern approximately agree well with the experimental data of the same 2θ range in (a).

$(Bi(Bi_2S_3)_9I_3)_{2/3}$ EDX mapping

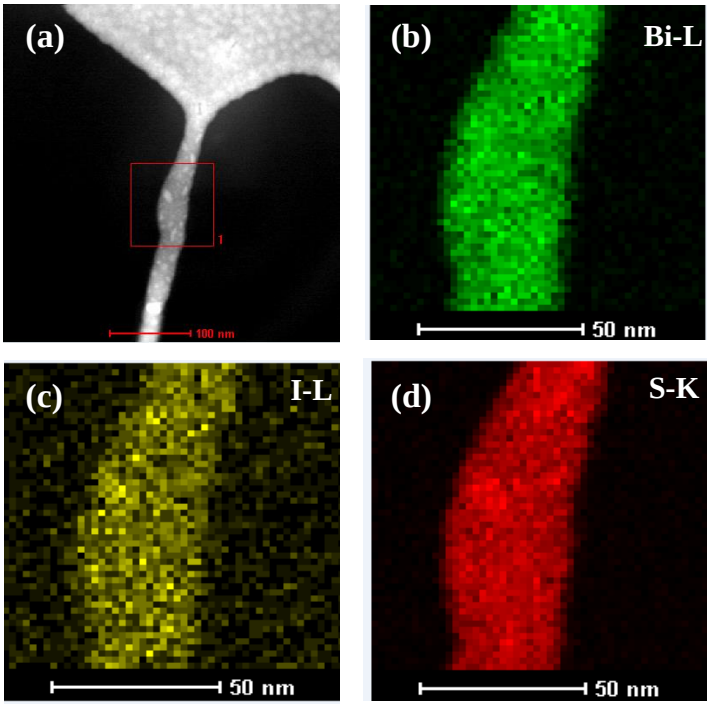

Element	Weight %	Atomic %
S(K)	17.509	54±3
I(K)	9.499	6±2
Bi(L)	78.991	40 ±2

$(Bi(Bi_2S_3)_9I_3)_{2/3} \sim Bi_{12.667}S_{18}I_2$

Expected: S ~ 55.1%
I ~ 6.1%
Bi ~ 38.8%

Fig. S2. The energy dispersive X-ray (EDX) mapping of $(Bi(Bi_2S_3)_9I_3)_{0.667}$ from HRTEM analysis. (a) The HRTEM picture of $(Bi(Bi_2S_3)_9I_3)_{0.667}$ after a focused-ion-beam cutting. The area for mapping the element content is displayed by a red square. (b) Green color mapping of Bi L line from the square in (a). (c) The composition of iodine is shown by yellow-color mapping with the I L line. (d) Red color mapping of S K line. The EDX analysis of atomic percentage of the as-grown crystal is 54±3 % for sulfur, 6±2 % for iodine, and 40±2 % for bismuth, respectively. The values are in good agreements with those of $(Bi(Bi_2S_3)_9I_3)_{0.667}$ corresponding to a $Bi_{12.667}S_{18}I_2$ stoichiometric content (i.e. S ~ 55.1 %, I ~ 6.1 %, and Bi ~ 38.8 %).

Figure S1(a) displays the experimental powder XRD pattern of the as-grown $(Bi(Bi_2S_3)_9I_3)_{0.667}$ by CVT. The powdered sample was obtained by finely ground the small bulk crystals of $(Bi(Bi_2S_3)_9I_3)_{0.667}$ into powder. The XRD pattern is similar to that of previous JCPDS card No. 73-1157 [18] and that of the needle-like crystals grown by polyol method.[17] The analysis of

XRD result in Fig. S1(a) reveals the lattice constants of $(Bi(Bi_2S_3)_9I_3)_{0.667}$ are a=15.71 Å and c=4.02 Å and crystal structure is hexagonal with a symmetry of space group P63/m. Detailed analysis of the structure, atomic coordination and stoichiometry using XRD are also included in APPENDIX 1. Figure S1(b) shows the simulation curve of XRD from 2θ=10° to 50° using the obtained structure and lattice parameters in Fig. S1(a). The relative intensity and peak pattern of the simulation curve show good agreement with the experimental data in Fig. S1(a). It verifies hexagonal structure of the $(Bi(Bi_2S_3)_9I_3)_{0.667}$ nano-/micro- rods grown by CVT.

To verify the stoichiometry of the as-grown $(Bi(Bi_2S_3)_9I_3)_{0.667}$ single crystals, the EDX experiment was also implemented. Fig. S2 shows the EDX analysis of the as-grown $(Bi(Bi_2S_3)_9I_3)_{0.667}$ nano rod from the HRTEM experiment. Fig. S2(a) shows the area of EDX analysis, Fig. S2(b) shows the Bi L-line mapping, Fig. S2(c) shows the I L-line mapping and Fig. S2(d) shows the S K-line mapping, respectively. The values of stoichiometric content of the nano rod are calculated to be 54±3 % for sulfur, 6±2 % for iodine, and 40±2 % for bismuth, respectively. The obtained stoichiometric compositions are corresponding to $Bi_{12.667}S_{18}I_2$, and which matches well with $(Bi(Bi_2S_3)_9I_3)_{2/3}$. The result also matches well with the XRD analysis in APPENDIX 1.

Optical characterization

Thermoreflectance (TR) experiments of the m-plane $(Bi(Bi_2S_3)_9I_3)_{0.667}$ were implemented using indirect heating manner with a gold-evaporated quartz plate as the heating element.[25,26] Prior

to the TR experiment, the sheet-type sample of the rod was polished from a thick rod into a thin sample. The thin m-plane sample was closely attached on the heating element by silicone grease. The on-off heating disturbance uniformly modulates the thin m-plane $(Bi(Bi_2S_3)_9I_3)_{0.667}$ periodically. An 150 W tungsten halogen lamp (or an 150 W xenon-arc lamp) filtered by a PTI 0.2-m monochromator provided the monochromatic light. The incident light is focused onto the sample with a spot size less than hundred μm^2. An InGaAs photodetector acted as the detection unit and the TR signal was measured and recorded via an EG&G model 7265 lock-in amplifier. For transmittance measurement, the same monochromatic system and light source as those of TR were used. The thickness of the m-plane $(Bi(Bi_2S_3)_9I_3)_{0.667}$ sample is about 50 μm. The incident monochromatic light was chopped (200 Hz), and the transmission signal was measured and recorded via an EG&G model 7265 lock-in amplifier that combined with the InGaAs photodetector. A closed-cycle cryogenic refrigerator with a thermometer controller facilitates the low-temperature measurements for transmittance and TR measurements.

The μRaman measurement of the m-plane $(Bi(Bi_2S_3)_9I_3)_{0.667}$ hexagonal micro rod was carried out by using a RAMaker integrated micro-Raman-PL identified system equipped with one 532-nm solid-state diode pumped laser as the excitation sources. A light-guiding microscope (LGM) equipped with one Olympus objective lens (50x, working distance ~8 mm) acts as the inter-connection coupled medium between the nano rod sample, incident and reflected lights, and charge-coupled-device (CCD) spectrometer. A pair of dichroic sheet polarizers (in visible to infrared range) was utilized for polarization-dependent measurements. The measurement

configuration of polarized μRaman is setting as $Z(XX)\bar{Z}$ and $Z(XY)\bar{Z}$ on the m-plane $(Bi(Bi_2S_3)_9I_3)_{0.667}$, where X is along the *c* axis of the hexagonal rod.

Supplementary Information Reference:

25 C. H. Ho, H. W. Lee, and Z. H. Cheng, *Rev. Sci. Instrum.* 2004, **75**, 1098-1102.

26 C. H. Ho and H. H. Chen, *Sci Rep.* 2014, **4**, 6143.

APPENDIX 1

==========

Table 1. Crystal data and structure refinement for 1.

Identification code	1
Empirical formula	Bi12.667 I2 S18
Formula weight	3547.62
Temperature	296(2) K
Wavelength	0.71073 A
Crystal system, space group	Hexagonal, P6(3)/m
Unit cell dimensions	a = 15.6203(6) A alpha = 90 deg. b = 15.6203(6) A beta = 90 deg. c = 4.0211(2) A gamma = 120 deg.
Volume	849.68(8) A^3
Z, Calculated density	1, 6.933 Mg/m^3
Absorption coefficient	69.960 mm^-1
F(000)	1473
Crystal size	0.400 x 0.060 x 0.040 mm
Theta range for data collection	1.505 to 28.271 deg.
Limiting indices	-20<=h<=20, -19<=k<=20, -5<=l<=5
Reflections collected / unique	6454 / 807 [R(int) = 0.0386]
Completeness to theta = 25.242	100.0 %
Absorption correction	None
Refinement method	Full-matrix least-squares on F^2
Data / restraints / parameters	807 / 0 / 37
Goodness-of-fit on F^2	1.138
Final R indices [I>2 sigma(I)]	R1 = 0.0205, wR2 = 0.0453
R indices (all data)	R1 = 0.0208, wR2 = 0.0455
Extinction coefficient	0.00113(8)
Largest diff. peak and hole	3.719 and -2.379 e.A^-3

Table 2. Atomic coordinates (x 10^4) and equivalent isotropic displacement parameters (A^2 x 10^3) for 1.
U(eq) is defined as one third of the trace of the orthogonalized Uij tensor.

	x	y	z	U(eq)
Bi(1)	8785(1)	4891(1)	7500	15(1)
Bi(2)	10556(1)	7591(1)	2500	20(1)
Bi(3)	10000	10000	-3944(5)	33(1)
I(1)	6667	3333	2500	16(1)
S(1)	9828(2)	8148(2)	-2500	13(1)
S(2)	8682(1)	6052(1)	2500	12(1)
S(3)	10669(1)	6128(1)	7500	12(1)

Table 3. Anisotropic displacement parameters (A^2 x 10^3) for 1.
The anisotropic displacement factor exponent takes the form:
-2 pi^2 [h^2 a*^2 U11 + ... + 2 h k a* b* U12]

	U11	U22	U33	U23	U13	U12
Bi(1)	12(1)	14(1)	18(1)	0	0	6(1)
Bi(2)	21(1)	29(1)	17(1)	0	0	18(1)
Bi(3)	27(1)	27(1)	45(1)	0	0	14(1)
I(1)	15(1)	15(1)	17(1)	0	0	7(1)
S(1)	13(1)	15(1)	13(1)	0	0	8(1)
S(2)	12(1)	12(1)	12(1)	0	0	6(1)
S(3)	11(1)	11(1)	12(1)	0	0	6(1)